IEEE Access
Multidisciplinary | Rapid Review | Open Access Journal

Received April 11, 2019, accepted April 23, 2019, date of publication May 1, 2019, date of current version May 16, 2019.

Digital Object Identifier 10.1109/ACCESS.2019.2914220

A Lightweight and Cost-Effective 3D Omnidirectional Depth Sensor Based on Laser Triangulation

YOUNGBIN SON[1], SEONGWON YOON[1], SE-YOUNG OH[2], (Senior Member, IEEE), AND SOOHEE HAN[1], (Senior Member, IEEE)

[1]Department of Creative IT Engineering, Pohang University of Science and Technology, Pohang 37673, South Korea
[2]Department of Electrical Engineering, Pohang University of Science and Technology, Pohang 37673, South Korea

Corresponding author: Soohee Han (soohee.han@postech.ac.kr)

This work was supported in part by the Sports Promotion Fund of Seoul Olympic Sports Promotion Foundation from the Ministry of Culture, Sports and Tourism under Grant 1375026841, and in part by the Human Resources Program in Energy Technology, Korea Institute of Energy Technology Evaluation and Planning, granted financial resource from Ministry of Trade, Industry and Energy, under Grant 20174030201660.

ABSTRACT In this paper, we propose a new lightweight and cost-effective 3D omnidirectional depth sensor based on laser triangulation in order to ensure a wide field of view (FOV) while achieving portability and affordability. The proposed sensor is tiny palm-sized and hence easily installed even on small moving objects, which is largely composed of a structured light-based 2D sensor and a rotating motor for creating a full 360 degree horizontal FOV, thus providing a 3D omnidirectional sensing capability. The structured light-based 2D sensor is specially designed to maximize the vertical FOV by employing a fisheye camera and a laser beam passing through two cylindrical lenses for projecting a line onto a surface. From the rotational movement of the 2D sensor due to the mounted motor, its surroundings are scanned by extracting the corresponding 3D omnidirectional depth information from laser triangulation. The actual implementation is carried out to examine the technical feasibility of realizing the proposed 3D omnidirectioanl depth sensor. It turns out that the proposed depth sensor covers over 97 % area of its surrounding sphere. It is also observed through experiments that the proposed 3D omnidirectional depth sensor has similar accuracy to that of a Velodyne HDL-32, 32-channel light detection and ranging (LIDAR) sensor, at a range of 5 *m* to 6 *m* while providing much wider vertical FOV and higher vertical resolution.

INDEX TERMS Omnidirectional depth sensor, structured light, field of view (FOV).

I. INTRODUCTION

Innovations in active depth sensing technology have played an important role in making recent advances in autonomous robotics. The demand of high performance active depth sensors is increasing as they become essential in implementing simultaneous localization and mapping (SLAM), path planning, and obstacle avoidance algorithms for autonomous robotics. Among several performance criteria for such sought-after active depth sensors, the field of view (FOV) has been considered very important for more optimal and safe path planning decisions since it determines how widely they can see at a time. Its physical limitation may lead to serious performance degradation and dangerous consequences. If a given FOV is not sufficiently large, SLAM algorithms may often fail in cluttered or plain environments with few features [1]. Path planning and obstacle avoidance algorithms also suffer from a small FOV since the obstacles out of the sensor's FOV may result in collision, especially in the active environments such as crowded corridors. In order to resolve such problems arising from insufficient FOV, active depth sensors must be designed to have a wide FOV. Furthermore, they are expected to be lightweight and cost-effective since a variety of their applications are recently being created to be portable and affordable.

As one of basic methods of widening FOV, multiple depth sensors with different orientations have been employed and assembled to work like a single depth sensor [1].

The associate editor coordinating the review of this manuscript and approving it for publication was Muhammad Imran Tariq.

Most commercially available depth sensors can be combined in this fashion, which provides cheap and easy setup by simply interfacing them physically. However, such approaches lead to a bulky size and heavy weight because of multiple depth sensors, additional fixtures and interface hardware putting them together. Moreover, the relative attitudes and positions between depth sensors should be initially calibrated to guarantee accuracy during operation. In this regard, a single depth sensor based approaches would be much more desirable for practical reasons.

For realizing a large FOV with a single depth sensor, catadioptric omnidirectional camera [2] based approaches have been also proposed. Active depth sensing based on a catadioptric omnidirectional camera has been tried out with a laser projector which emits cone or plane shaped beams [3], [4]. This approach can obtain the depth information based on laser triangulation with a 360 degree horizontal FOV, but it can measure the depth only on the projected beam contour at rest, or when it is not moving. Accurately speaking, such an approach is intended for 2D depth sensing instead of 3D one. Its improved versions for 3D depth sensing have later been introduced by distinctive beam patterns [5], projecting discretely-multiple [6], and continuously-multiple cone-shaped beams [7]. Since these approaches employ two separate mirrors for a camera and a laser projector, a bulky and heavy design cannot be avoided. For lightweight design, a method with one mirror shared by a camera and a laser projector has also been proposed, which is not verified by practical implementation [8]. Even though the aforementioned catadioptric mirror based approaches try to achieve a large horizontal FOV with a single depth sensor, they still have an inherent limitation on the vertical FOV due to their inevitable blind spots from cameras and mirrors, and due to inferior accuracy of the laser triangulation at the edge of images.

In order to achieve a wide vertical FOV with long range and high accuracy, another interesting approach has been taken with actuated light detection and ranging (LIDAR) sensors that can be variously configured to be spinning (rolling) [9], nodding (pitching) [10], and arm-controlled [11]. This approach can be also applied to a fully omnidirectional depth sensing system with infinitely pitching mechanism [12]. Owing to the flexible configuration of LIDAR sensors, such omnidirectional sensing methods have been applied to a variety of applications such as indoor robotic SLAM [13], micro aerial vehicles (MAVs) navigation [14], human-robot interaction (HRI) [15], and so on. Even though the actuated LIDAR based approach provides a fully omnidirectional depth sensing capability, it has a limitation of having extremely coarse resolution along its actuated direction, making it difficult to apply to dynamic environments. Besides, this LIDAR approach is unfavorable to cost, size, and weight.

Looking into the aforementioned depth sensors, it would be meaningful to develop a 3D omnidirectional depth sensor that has a large vertical and horizontal FOVs, and a sufficiently fine horizontal resolution while being cost-effective and lightweight. In this paper, we propose a lightweight and cost-effective 3D omnidirectional depth sensor based on laser triangulation in order to ensure a wide FOV while achieving portability and affordability. As a single depth sensor without using heavy and bulky components such as mirrors, the proposed sensor is palm-sized and hence easily mounted even to small moving objects. It largely consists of a structured light based 2D depth sensor and a rotating motor for creating a full 360 degrees horizontal FOV thus providing a 3D omnidirectional sensing capability. The structured light based 2D depth sensor is specially designed to maximize the vertical FOV by employing a fisheye camera and a laser beam passing through a cylindrical lens for projecting a line onto a surface. If a camera with high frame rate is employed, the horizontal resolution can be finer than that of LIDAR sensors. From the rotational movement of the 2D sensing with the motor, its surroundings are scanned by extracting the corresponding 3D omnidirectional depth information from laser triangulation. It is shown through experiments that the proposed 3D omnidirectional depth sensor covers over 97 % area of its surrounding sphere. It is also observed that the accuracy of proposed 3D omnidirectional depth sensor is similar to that of a Velodyne HDL-32, a 32-channel LIDAR at typical working range of the proposed sensor while providing much wider vertical FOV and higher vertical resolution.

To sum up, the design objective of the proposed sensor is firstly to provide a very wide FOV in both horizontal and vertical aspects while being portable and affordable, and secondly to achieve a similar 3D depth sensing capabability compared with other existing 3D depth sensors. In Table 1, some 3D depth sensors including the proposed one are compared and ranked in the order of ⊙ > ∘ >△> x by means of the corresponding criteria. Horizontal and vertical FOVs of multiple depth sensors are configurable since they are dependent on how many sensors are involved. As the number of their depth sensors increases, their FOV will get larger, but their weight and size grow heavier and bigger at the same time. There is a trade-off between the FOV and the lightweight and compact design.

This paper is organized as follows: Details on hardware implementation are described in Section II. Section III describes how to compute the depth from 2D measurements. The accuracy of the proposed 3D omnidirectional depth sensor is illustrated with real experiments and compared with a 32-channel Velodyne LIDAR sensor in Section IV. Various issues on the sensor implementation are discussed in Section V. Finally, the advantages of the proposed work are summarized and a conclusion is drawn in Section VI.

II. HARDWARE IMPLEMENTATION

The full view of the proposed 3D omnidirectional depth sensor is shown in Fig. 1. Functionally, the proposed sensor is largely divided into two components: 2D sensing and 3D depth sensing. 2D sensing is achieved vertically from a line laser and then omnidirectional 3D depth sensing is provided by the triangulation method and a horizontal rotating

TABLE 1. Comparison with other 3D depth sensors.

Sensor type	Multiple depth sensors	Single depth sensor		
Design	Multiple RGB-D sensors	Catadioptric mirror based sensor	Actuated LIDAR	Proposed sensor
Cost	△	△	x	○
Size	x	○	○	○
Weight	x	○	△	○
Horizontal FOV	Configurable	○	○	○
Vertical FOV	Configurable	△	◎	○
Horizontal resolution	◎	○	x	△
Vertical resolution	◎	△	○	○
Accuracy	○	△	◎	○
Range	○	△	◎	○
Instant Measurement	○	○	x	x

◎, ○, △, and x are arranged in favorable order.

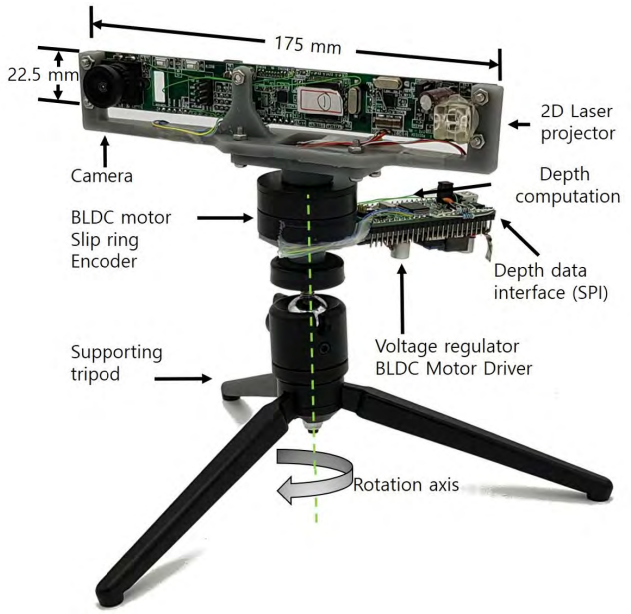

FIGURE 1. The proposed 3D omnidirectional depth sensor mounted on a supporting tripod.

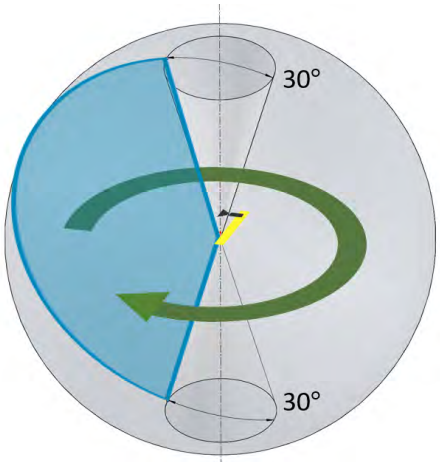

FIGURE 2. Sensing coverage of the proposed 3D omnidirectional depth sensor.

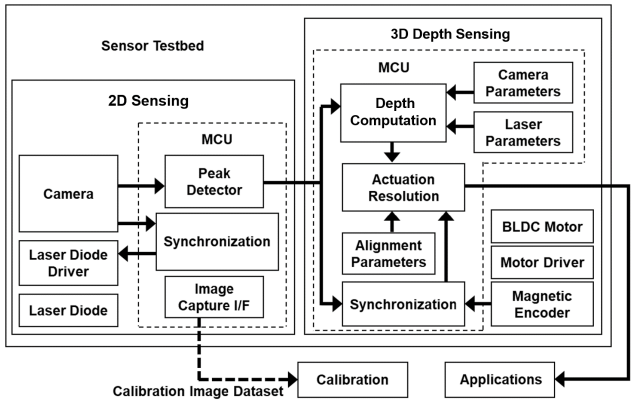

FIGURE 3. A block diagram of the overall architecture of the proposed 3D omnidirectional depth sensor.

motion of a BLDC motor. As seen in Fig. 2, the proposed sensor can scan the surrounding environment in all directions, providing the sensing coverage of over 97 % over the entire surrounding area. This is why the proposed sensor is called omnidirectional. In Section IV, its wide coverage will be verified with experiments. To the best of the authors' knowledge, there is no commercial off-the-shelf (COTS) or prototyped sensor that has such a wide sensing coverage and lightweight implementation using only cost-effective components. The proposed sensor in Fig. 1 weighs 170 g and its size is 210 × 80 mm (diameter x hight), including a BLDC motor. It is powered by 12 V direct current (DC) voltage and a nominal current of 0.6 A with a peak of 1.1 A at motor startup. Key components adopted for the proposed 3D omnidirectional depth sensor are described in Table 2.

A block diagram of the function modules of the proposed sensor is depicted in Fig. 3. It has two ARM Cortex-M4F based cost-effective microcontroller units (MCUs) installed for 2D sensing and the depth computation, respectively, operating at 168 MHz. The MCU for 2D sensing takes cropped images from the camera and localizes the peak of the power distribution among the pixels of each row to detect exact peaks from the blurred line laser with sub-pixel accuracy. The localized peaks are transmitted over a serial peripheral interface (SPI) connection to the other MCU for depth

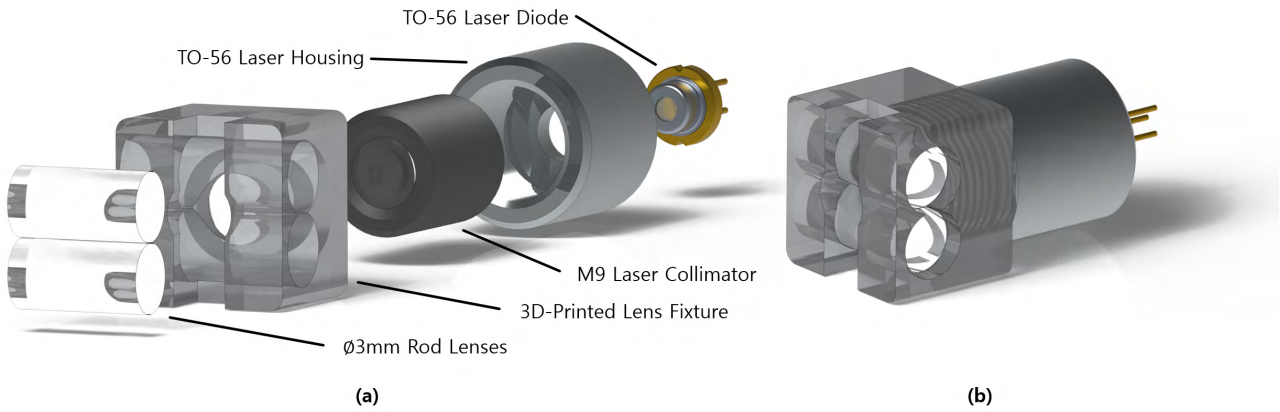

FIGURE 4. An exploded view (a) and an assembled view (b) of the proposed line laser projector assembly.

computation. The large box shown on the right in Fig. 3 includes functions that deal with the received localized peaks. By the subpixel edge detection and the triangulation method, the localized peaks are processed into 3D point cloud data in the body coordinate system. From the angular position measured from an encoder of the installed BLDC motor, 3D point cloud data is transformed to the sensor coordinate system and then the result is delivered to user applications over a serial communication interface. Furthermore, an Ethernet-based debug interface is also provided to take full-frame images. By using the full-frame images, calibration procedures for tuning intrinsic and distortion parameters of the camera sensors are carried out with a specialized model [16] to enhance the sensing accuracy. The full-frame images are also used in calibrating laser projector parameters for triangulation procedure.

More details on two components for 2D sensing and 3D depth sensing will follow.

A. 2D SENSING WITH A LINE LASER

A triangulation method determines the unknown location of a certain point by forming a spatial triangle together with two other known points. Most structured light based sensors for 3D scanning employ the triangulation method to reconstruct depth information from 2D measurements. Typically, the triangulation method has been applied to a lens based camera and a prism based laser projector for scanning external objects with a moderate FOV. As mentioned in Introduction, in order to obtain a large FOV, the triangulation method with a catadioptric camera and a conic mirror based laser projector has also been tried, but it requires expensive and heavy design [3]. For the first time, this paper applies the triangulation method to a fisheye lens based camera and a prism based laser projector, combination of which provides a compact, cost-effective, and lightweight design while achieving a large FOV up to 150 degrees in 2D sensing. Severe distortion arising from the fisheye lens can be compensated from well-known subpixel edge detection schemes and an appropriate camera model [16], [17]. Details on the triangulation procedure are given in Section III.

The implemented hardware for 2D sensing with a line laser weighs 46 g and its size is 175 $\times$ 22.5 mm, including an on-board Ethernet, USB and JTAG debug ports, and various headers for debugging purpose. The baseline length between the camera and the laser projector was chosen to be 150 mm. A 450 nm band-pass filter for rejecting ambient light is installed between the fisheye lens and the image sensor. A commercial-off-the-shelf universal laser diode enclosure for the TO-56 laser diode and M9-threaded collimating lens is employed. The enclosure and the laser diode are both soldered to the PCB for enhancing heat dissipation capability.

A Stereolithography (SLA) 3D printable laser optic fixture is custom designed to generate a line laser with the widest possible fan angle (Fig. 4(a)). To firstly produce a point laser beam, an M9-threaded enclosed single collimating lens is screw-fixed to the M9-threaded hole of the fixture. Secondly, to produce the line laser, two ø3 mm cylindrical lenses are inserted and glue-fixed to the fixture. Finally, this optic assembly can be fasten to the enclosure by the screw-fix (Fig. 4(b)). In order to focus the laser, to align the line direction, and to avoid plastic optics deforming during the welding process, the actual assembly order should be followed as firstly welding the laser diode enclosure to the PCB, secondly screwing, focusing and gluing the collimating lens to the enclosure, finally screwing, aligning and gluing the line-laser-generating optic assembly to the collimating lens. We used a typical 30-minute epoxy glue to keep each component in its position. The fan angle of the generated line laser is observed to be greater than 150 degrees. The thickness of the line laser is measured by a ruler at various distances (Table 3). By analyzing this data, beam divergence is observed to be about 1.5 $mrad$, which is similar to those of typical laser pointers.

As seen in Table 2, a wide video graphics array (WVGA) (752 $\times$ 480 $pixels$) grayscale image sensor is adopted to take images at 297 frames per second (FPS) with shutter time

TABLE 2. The major components adopted for the proposed 3D omnidirectional depth sensor.

Function	Component	Manufacturer	Model	Description
2D sensing	Microcontroller	ST Microelectronics	STM32F407VET6	Cortex-M4F, 168 MHz
	Image sensor	ON Semiconductor	MT9V034C12STM	1/3" 752 × 480 Grayscale CMOS
	Laser diode	OSRAM	PL TB450B	$\lambda = 450\ nm$, 1.6 W
	Prism	Generic	N/A	Cylinder type, K9 glass ϕ=3 mm
	Lens	Generic	N/A	S-mount, f=1.38 mm, F2.8 Fisheye
	Filter	Generic	N/A	$\lambda = 450\ nm$, FWHM 10 nm
3D reconstruction	Microcontroller	ST Microelectronics	STM32F405RGT6	Cortex-M4F, 168 MHz
	Motor assembly	N/A	GB3505	24N22P Gimbal direct drive, Slip ring/encoder integrated
	Encoder	ams	AS5048A	
	Motor driver	Oversky	MR-20A	Sensorless BLDC motor driver

TABLE 3. Thickness measurement of the line laser at various distances with approximate accuracy of ±0.5*mm*.

Distance(m)	0.60	1.20	1.80	2.40	3.00	3.53	4.06	4.59	5.12	5.65
Half width(mm)	1	1	1.5	1.5	2	2.5	3	4	4	4.5

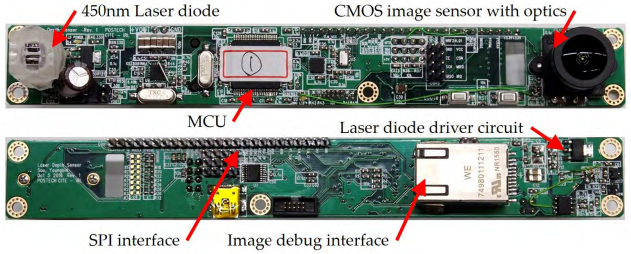

FIGURE 5. A structured light based 2D sensor.

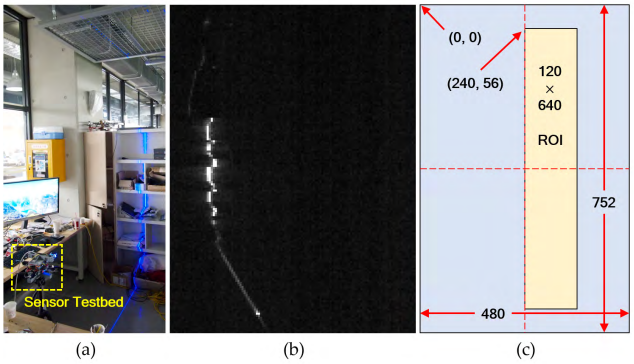

FIGURE 6. (a) An original image obtained from the proposed sensor (b) An preprocessed image with the extracted laser line (c) Region of interest placement on the surface of an image sensor.

of 200 μs. The laser diode driver and the strobe signal of the camera are synchronized at the moment of laser irradiation. The sensor is rotated by 90 degrees to keep portrait orientation and hence takes advantage of higher vertical resolution. Originally, the CMOS image sensor employed gives 60 FPS at full resolution. However, by resizing the image to a new width and height of the region-of-interest (ROI) or 120 × 640 *pixels* as seen in Fig. 6(c), about 5 times faster frame rate is achieved within the rated clock. Additionally, a native row-wise 4-binning strategy is applied to reduce undesirable noise of the image, which reduces the image size by 4 times to 120 × 160 *pixels*. As seen in Fig. 6(b), the image is stored and rotated on the MCU. Finally, the preprocessed image is fed into the peak detection algorithm that detects edges in each row with sub-pixel accuracy. Extracted peak positions are passed over the SPI to the 3D depth sensing component.

Most triangulation methods have ambient light rejection ability to avoid failure in high ambient light. For ambient light rejection, the difference image method is often employed, which makes use of two consecutive images at a fixed pose. One of the two consecutive images is taken with laser turned on and the other with laser turned off. The image taken with laser turned on is subtracted by the other, which removes ambient light from a scene, leaving the line laser only. However, the proposed sensor system continuously rotates the 2D sensor seen in Fig. 1, which makes it impossible to adopt the difference image method conducted at a fixed pose. Therefore, the implemented sensor may suffer from ambient light such as the fluorescent light. However, this problem can be easily solved by employing an infrared (IR) laser and a corresponding band-pass filter properly. For easy development and safe experiment, a visible wavelength laser is employed in this paper. The IR laser could be employed for commercial product development.

For high resolution and real time laser line detection from 2D raw pixel data measured in the image sensor, this paper employs an efficient peak detection algorithm, called the Gaussian approximated laser peak method [17], since it is known to have good performance and affordable computation burden with cost-effective MCUs. Letting m'_r and δm_r be the indices of the maximum intensity pixel and the subpixel offset in r-th row, respectively, we have the indices m_r of the subpixel peaks as follows:

$$\delta m_r = 0.5\frac{\ln(i_r(m_r-1)) - \ln(i_r(m_r+1))}{\ln(i_r(m_r-1)) - 2\ln(i_r(m_r)) - \ln(i_r(m_r+1))}$$
$$m_r = m'_r + \delta m_r$$

where $i_r(x)$ is the intensity of the x-th pixel in r-th row. Since the intensity values are integers ranging from 0 to 255,

or 8-bit grayscale, a 256-word-long look up table (LUT) was used to mitigate the heavy computation burden required for calculating logarithm accurately.

B. 3D DEPTH SENSING WITH A TRIANGULATION METHOD AND A ROTATING MOTOR

For omnidirectional 3D sensing with 2D images preprocessed by the edge detection algorithm of the structured light based 2D sensor, the proposed sensor employs a triangulation method and a rotating motor. Since details on the triangulation method will be given in the next section, we discuss a rotating motor only in this section. A COTS brushless DC (BLDC) motor and a motor driver are used to rotate the 2D sensor. The implemented motor system provides a rotation velocity from 3 *Hz* (1080 degrees/*sec*) to 10 *Hz* (3600 degrees/*sec*). Since the motor being used (Table 2) is mainly for camera gimbal control, an enhanced motor controller with angular position control capability may be adopted to densify scans per each revolution and then improve horizontal resolution if needed. A magnetic encoder built into the motor is used to measure the angular position of the motor. Subpixel accuracy peak locations from the structured light based 2D sensor, the strobe signal of the camera, and the necessary power are delivered through a slip ring attached to the motor. Since even very small angular position estimation errors may result in a very poor depth resolution, angular and peak positions coming from the encoder and the 2D sensor, respectively, are well synchronized on a real time basis before entering the triangulation procedure. A system timer integrated with an MCU is used for synchronization, providing temporal information with precision down to a few microseconds. Furthermore, angular positions at an arbitrary time are interpolated with the previously measured one and the angular rate to overcome the slow sampling rate (1 *kHz*) of the magnetic encoder and then achieve the high accuracy up to a certain point. To estimate the angular rate, a simple 4-tap averaging filter is applied to the most recent angular position data. The measurement delay of the magnetic encoder is also empirically found and accommodated for estimating the angular rate. After receiving the strobe signal of the image sensor, the angular positions at the moment of the time stamping strobe signals are estimated and their estimates are tagged to the peak position data before proceeding to the triangulation procedure.

III. DEPTH COMPUTATION

A. COORDINTATE FRAME

As mentioned in the previous section and seen in Fig. 7, the proposed omnidirectional 3D depth sensor consists of a structure light based 2D sensor and a rotating motor. Since the camera is some distance away from the laser projector and the 2D sensor is rotated by the motor, some coordinate systems are needed to provide tractable computation. As seen in Fig. 7, four coordinate systems are chosen for modeling the proposed sensor. Firstly, a 3D Cartesian sensor coordinate

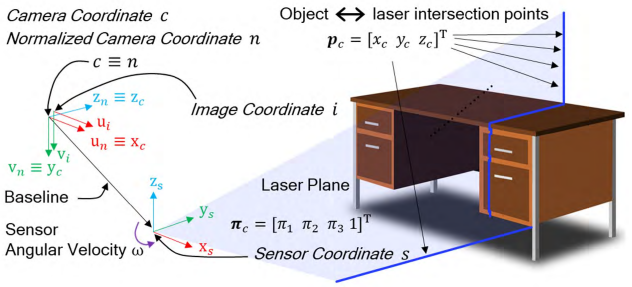

FIGURE 7. Four coordinate systems adopted for the proposed 3D omnidirectional depth sensor.

system *s* is rigidly attatched to the motor mount of the 2D sensor. *s* has its origin at the sensor mounting hole with its *z*-axis aligned to the rotation axis of the motor and its *y*-axis facing toward the front side of the sensor. Secondly, a 3D Cartesian camera coordinate system *c* is rigidly fixed to the camera of the 2D sensor. The origin and axes of the 3D Cartesian camera coordinate system also provide the third coordinate system, called the normalized image coordinate system *n*, that is constructed to describe the projection geometry with its origin at the focal point of the fisheye lens and its *z*-axis aligned to the optical axis of the camera. Finally, the 2D image coordinate system *i* is defined on the CMOS image sensor.

B. TRIANGULATION PROCEDURE

The triangulation procedure starts from taking the laser peak points which are described in the image coordinate system *i*, and returns the 3D point cloud described in the sensor coordinate system *s*. The triangulation procedure can be largely divided into 3 steps: a normalization step, a triangulation step, and a resolution step. The normalization step transforms the coordinate system of the detected laser peak points from *i* to *n*, using a camera model calibrated for fisheye lens [18]. The triangulation step triangulates the peak points by inversely projecting the 2D peak points into a 3D camera coordinate to calculate the intersection of the projected ray and the laser plane. The resolution step transforms the coordinate system of the point clouds from *c* to *s*.

In order to maximize the 3D omnidirectional depth sensing capability, it is essential to achieve a large vertical FOV, or fan angle, of the line laser. First of all, in this paper, a fisheye lens with a sufficiently large FOV of 185 degrees is employed to adequately accommodate the FOV of the line laser even though its images suffer from the quality deterioration at the extreme edges. A specialized camera model [18] is adopted instead of a pinhole camera model and a commonly used radial distortion model [19] in order to minimize the accuracy degradation due to fisheye lenses in conducting triangulation. It is shown through experiments that a real vertical FOV of the line laser generated from the implemented laser projector does not reach 180 degrees, but about 150 degrees, and thus each uppermost and bottommost portion of the line laser has an unusable FOV of about 15 degrees.

The camera model transforms a point $p_i = [u_i\ v_i]^T$ on the image sensor coordinate i to a point $p_n = [u_n\ v_n\ 1]^T$ on the normalized image coordinate n. The image sensor coordinate i can be considered as a 2D coordinate while the normalized image coordinate n as a homogeneous 2D coordinate. Transformation from p_i to p_n can be written as

$$p_n = \begin{bmatrix} (A^{-1}(p_i - t))^T \\ f(A^{-1}(p_i - t)) \end{bmatrix}, \tag{1}$$

where $A \in \Re^{2\times 2}$ is the affine transformation matrix, $t \in \Re^{2\times 1}$ is the offset vector, and $f(\cdot)$ is the nonlinear imaging function for modeling the imaging behavior up to M-th order as follows:

$$f(\begin{bmatrix} u \\ v \end{bmatrix}) = \sum_{k=0}^{M} a_k (u^2 + v^2)^{0.5k}. \tag{2}$$

It is noted that M is typically chosen between 4 and 8. In this paper, M is taken to be 6. The affine transformation matrix A and the offset vector t in (2) can be computed off-line in advance.

Assuming the normalized image coordinate n reduces to the 3D Cartesian camera coordinate c, we have

$$p_n = \begin{bmatrix} u_n z_c & v_n z_c & z_c \end{bmatrix}^T = p_c = \begin{bmatrix} x_c & y_c & z_c \end{bmatrix}^T, \tag{3}$$

for $z_c > 0$ to be determined later on, where $p_c = [x_c\ y_c\ z_c]^T$ is a point in c. From (3), p_n can be considered as an inverse projection ray. The goal of triangulation is to find the intersection of p_n and the laser plane described as

$$\pi_1 x + \pi_2 y + \pi_3 z + 1 = 0, \tag{4}$$

on the camera coordinate system c. Intersection of the inverse projection ray p_n and the laser plane can be obtained by solving

$$\begin{bmatrix} u_n z_c & v_n z_c & z_c & 1 \end{bmatrix} \begin{bmatrix} \pi_1 & \pi_2 & \pi_3 & 1 \end{bmatrix}^T = 0, \tag{5}$$

which yields the following solution:

$$p_c = \begin{bmatrix} x_c \\ y_c \\ z_c \end{bmatrix} = \frac{1}{\pi_1\, u_n + \pi_2\, v_n + \pi_3} \begin{bmatrix} -u_n \\ -v_n \\ -1 \end{bmatrix}. \tag{6}$$

Finally, the resolution step is carried out to represent p_c in the sensor coordinate system s. Such transformation is achieved with the following translation vector and rotation matrix:

$$p_s = R_{c\to s}(p_c + T_c^s) \tag{7}$$

where $R_{c\to s} \in \Re^{3\times 3}$ is the time-varying transformation matrix due to the rotation of the motor and $T_c^s \in \Re^{3\times 1}$ represented in c is the translation vector starting from the origin of c and pointing to the origin of s. $R_{c\to s}$ and T_c^s can be obtained from encoder data and physical positions of the sensor mounting hole and the camera.

IV. VERIFICATION

This section provides experimental results with the proposed 3D omnidirectional depth sensor. Fig. 8(a) shows that distances from the given origin to certain given points are measured exactly by recovering extrinsic parameters of the camera with a checkerboard and they are compared with the estimated distances computed by the proposed sensor. The errors between distances and their estimates are drawn in color and smoothed in surfaces (Fig. 8(b)). It is observed that mostly the depth estimation errors are below 10 *cm* within the range of 4 *m* and about 20 *cm* to 30 *cm* beyond 5 *m*. The vertical FOV of the 2D sensor in the proposed omnidirectional 3D depth sensor is observed to be about 150 degrees, where uniform estimation errors are observed up to a certain point within 4 *m*. It could not be considered much inferior to previous researches such as rotating point-laser triangulation scanner [20] showing the errors of 5*cm* and 20*cm* at 4*m* and 5.8*m* away, respectively, and line-laser triangulation scanner [21] showing the errors of 8*cm* and 25*cm* at 4*m* and 5.8*m* away, respectively. In Fig. 9, a small room is used for showing the accuracy of the proposed omnidirectional 3D depth sensor. It can be seen from Fig. 10 that the performance of the proposed omnidirectional 3D depth sensor is very similar to that of a 32-channel Velodyne LIDAR. Each object in Fig. 10 shows a desk, a bed, and a bookshelf in front, partially or fully. The proposed sensor measured the distance between the ceiling and the floor to be 2.216*m* (averaged) that is comparable to 2.199*m* of a Leica DISTO D2 laser distance meter (5-point averaged). Circular blind spots can be also seen in Fig. 10(a) and (d). It is remarkable that the proposed 3D omnidirectional depth sensor is not much inferior to a somewhat heavy and expensive Velodyne sensor even though the former is far smaller sized and more lightweight, and much less expensive than the latter.

V. DISCUSSION

A. FOCUSING THE LENSES

Different from typical line laser scanning systems which have a narrow working distance envelope, the proposed scanning system has a much wider working distance envelope, from about 0.2 $\sim$ 5 *m*. It is typically hard to fully accommodate such range within depth of field of the fixed-focus camera. Since the sensitivity of the image sensor of the camera must be maximized in order to cover a longer distance, the lens must be set to its maximum sized aperture possible, making it prohibited to increase the depth of field. It is thus important to appropriately set the focus of the camera to help the peak detector to accurately locate the peak points, because the accuracy of peak point detection heavily affects accuracy of depth computation. Therefore, we used a focusing strategy of setting the focus to the farther region of the working envelope. This seems to be reasonable considering the nature of triangulation based depth sensing schemes in which the peak detection error at a long range results in a greater depth error whereas the same at a close range rather results in smaller depth error. In our proposed

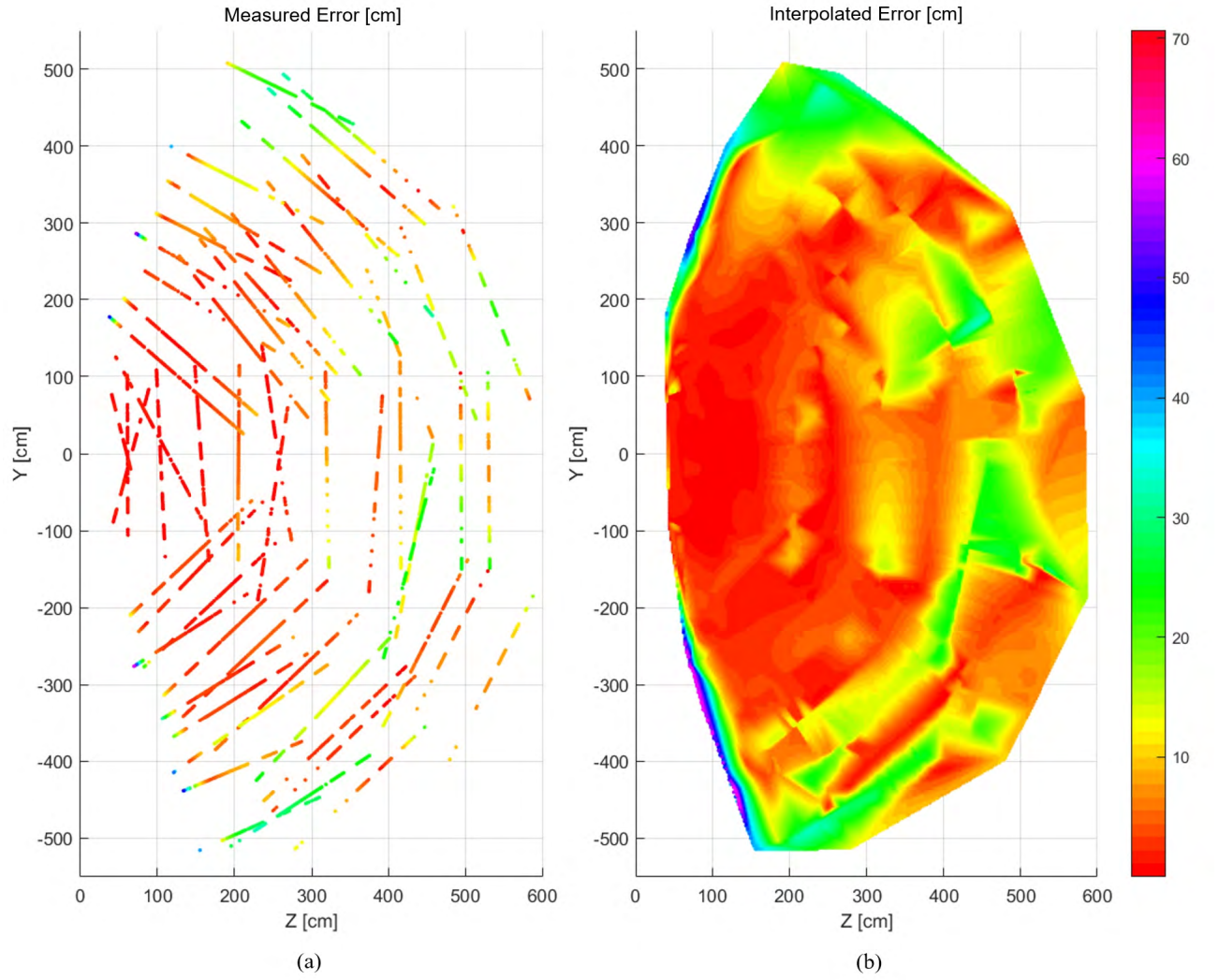

FIGURE 8. (a) Absolute depth estimation error in *YZ*-plane of the camera coordinate system (b) A smooth surface using piecewise cubic interpolation.

FIGURE 9. A horizontal panoramic view of a small room for sensor evaluation.

implementation, by focusing the lens at points 1 m away, the depth of field of the camera ranges from about 0.5 m to ∞.

Focusing the laser source is deemed to have less importance than focusing the camera. A typical focusing accuracy ($1 \sim 2$ *mrad*) of cheap laser pointer is sufficient. The divergence of the line laser over its shorter axis (perpendicular to the line laser) in the proposed implementation is about 1.51 *mrad*, which is similar to that of commercial laser pointers. Since the approximate angular resolution of the camera is about 4.1 *mrad*/*pixel* (3.14°/752 *pixel*), even a poorly focused laser of 5 *mrad* can be fit into a 3-pixel-wide subpixel peak detection window. More importantly, the centroid of the peak region still remains at its original laser plane and hence can be accurately located by the subpixel accuracy peak detector.

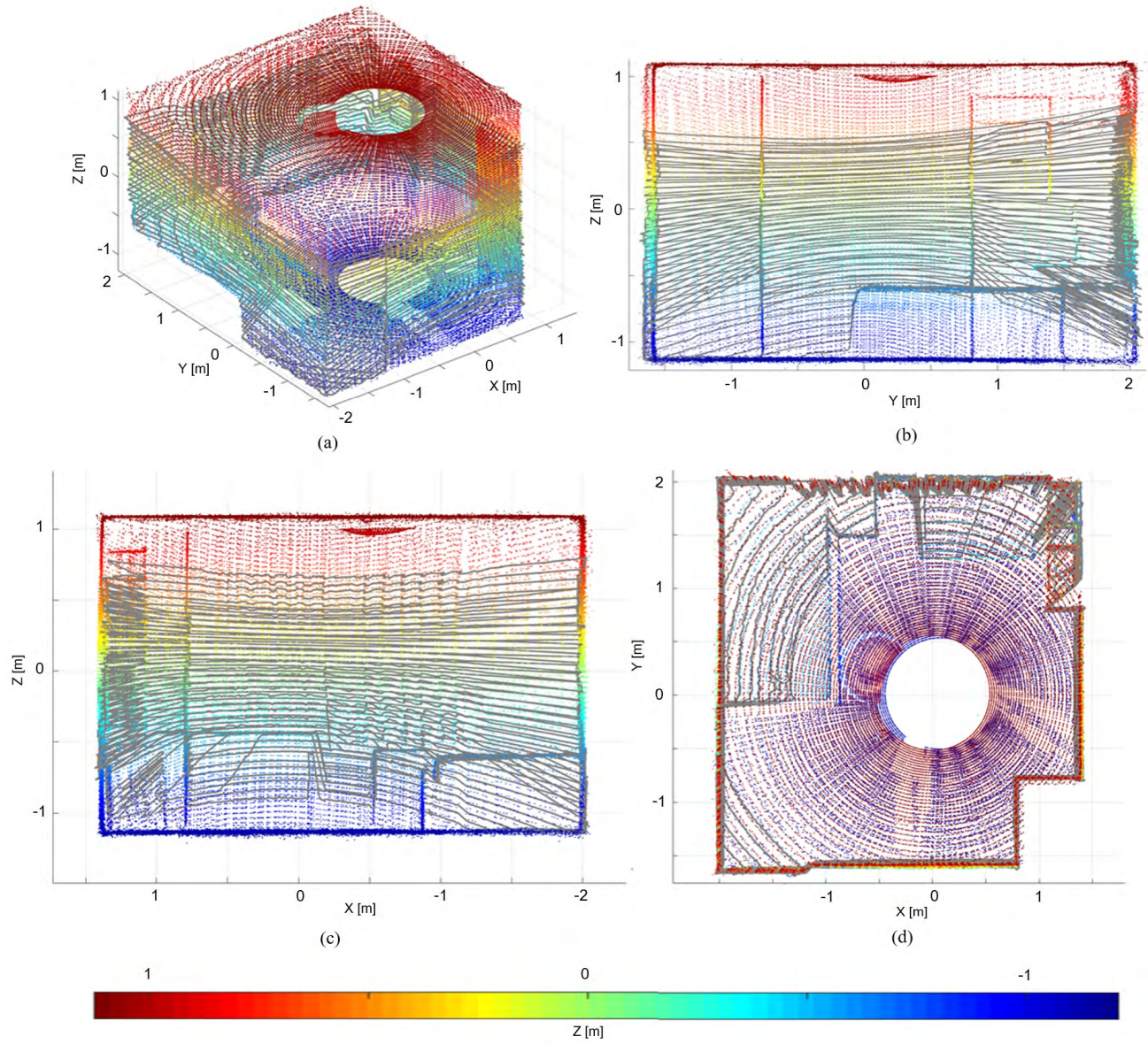

FIGURE 10. 3D and projected 2D(*YZ*, *XZ*, *XY*) images of point clouds obtained from the proposed 3D omnidirectional depth sensor(height-color coded) and a 32 channel Velodyne LIDAR sensor(gray colored).

B. BASELINE SELECTION

Since the proposed sensor utilizes triangulation technique to estimate depth, baseline length between the camera and the line laser can be lengthened to achieve higher accuracy. However, to do so, it is clear that the volume of the sensor becomes larger. Based on the fact that both volume and accuracy of the proposed sensor are major attributes, care must be taken to choose the baseline length. Assuming a pinhole camera based line laser sensor with its laser plane orthogonally placed to its baseline vector, it is well known that depth computation error for an arbitrary distant object is inversely proportional to baseline length. Since proposed sensor utilizes a fisheye camera which gives highly distorted image, pinhole camera assumption cannot be exactly satisfied, but generally this rule can be applied.

Above rule can be used for relative accuracy comparison between baseline length selections. Therefore, since the trend of error have been derived, it can be used to determine baseline length for new implementations afterwards. However, in the authors' aspect, it could not be used for an initial baseline length determination because the authors could not predict the actual depth computation error (Fig. 8) before implementing it. A rule-of-thumb on determining baseline length based on target working range have been coined [22], describing depth can be reliably estimated if the depth is less than 40 times of baseline length. Based on this rule-of-thumb,

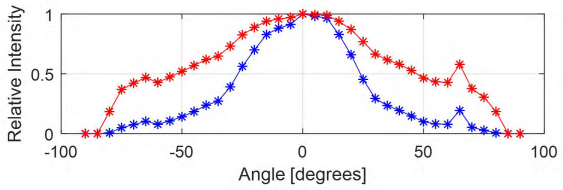

FIGURE 11. Intensity characteristic of the implemented line laser projector. (Blue) Relative intensity at an illuminated object. (Red) Estimated variation of maximum scanning range.

the authors chose the baseline length of 150mm, derived on targeted range of 6-meters.

C. LASER OPTICS CHARACTERISTICS

Since cylindrical line laser generation lens is used, line laser has nonuniform intensity distribution over its longer axis. Evaluation of the line laser generation optics have been done by measuring relative intensity along its projected line by using an optical power meter (Sanwa Electric Instrument LP1) (Fig. 11). The intensity of the darkest region ($\pm 75°$) of the line laser has only 5% of that of the brightest region ($\pm 0°$) of the line laser. This impacts on the maximum range of the sensor mainly, and additionally sensitivity of the sensor.

The main effect of such nonuniform intensity distribution is the restriction of scanning range. Since the powers per unit area of a line laser and its diffuse reflected one decreases over the distance linearly and quadratically, respectively, the relative sensitivity over a line laser can be regarded to be proportional to the cubic root of the relative intensity. Therefore, maximum scanning range on the darkest region ($\pm 75°$) of the line laser is about 33% of that of on the brightest region ($\pm 0°$). Secondly, nonuniform intensity distribution prohibits sensor to detect far objects at the both extreme of the line laser, if the object is dark (e.g. dark carpet floor at the extremes was not detected at $\geq$ 4m).

Although the implemented sensor integrates a 1600mW laser diode, measured laser output of the laser assembly is about 0.4 to 0.6W. This can be assumed as it is caused by reflections inside the lens assembly and lack of feedback photodiode (currently the laser diode is only driven by a current source).

D. CONSIDERATIONS FOR ACTUATOR IMPLEMENTATION

Because of the rotational movement, appropriate implementation of the actuator is crucial for the accuracy of the proposed 3D sensing mechanism. Major sources of accuracy degradation arising from mechanical issues can be categorized into three causes: (1) sensor-actuator misalignment, (2) angular position measurement error and (3) mechanical vibration. The former two problems may mainly affect the accuracy of the proposed sensing scheme. The final problem (3) may occur in the sensor element installed off center of a rotational body, which is often considered negligible. Compared to commercially available mechanical LIDARs such as Velodyne LIDARs which suffers from mechanical vibrations, the proposed sensor does not experience mechanical vibration significantly thanks to its light weight and compact size.

Rotational and translational sensor-actuator misalignments induce bias errors, distorting the captured scenes. Such errors cannot be avoided since it is almost impossible to achieve the exact alignment between the coordinates of a sensor and an actuator. To mitigate these errors, previous researches on the actuated LIDAR approaches have introduced various misalignment compensation algorithms such as fitting the captured scene to a known 3D model [23] and maximizing the crispness of the captured scene [12]. In the case of the proposed implementation, only the pitch angle misalignment has been manually corrected by inserting a few sheets of thin coating film between the PCB and the actuator frame. Misalignment on the roll angle is negligible because of the long aspect ratio of the sensor. A few millimeters translation misalignment is also negligible since the depth estimation error of the sensing element itself is in the order of centimeters. Yaw misalignment does not introduce distortion and hence is ignored.

Angular position measurement error mainly arises from inaccuracy of encoders. Magnetic encoders such as the one used in the proposed sensor have a very fine resolution and are compact, but they suffer from nonlinearity problems (up to 0.8°, corresponding to 8 *cm* of the depth estimation error at 5 *m* away). Alternatively, an optical encoder has a relatively coarse resolution but does not suffer from nonlinearity problems. Therefore, such a encoder may be employed to mitigate the nonlinearity problem with appropriate interpolation (which is already implemented on the proposed sensor) to overcome the lower resolution. It could be said that this type of encoders is preferable on the proposed sensing scheme because the sensing element always rotates at high rate during the nominal operation.

VI. CONCLUSION

In this paper, we proposed a new lightweight and cost-effective 3D omnidirectional depth sensor with structured light in order to obtain a wide FOV while satisfying other performance metrics such as accuracy. A line laser with a large fan angle is generated by passing the laser beam through two cylindrical lenses and it scans the surrounding environment by rotational motion of a BLDC motor. No large, heavy, or expensive components are required for implementation. The size and weight of the proposed 3D omnidirectional depth sensor are significantly reduced compared with those of existing similar 3D depth sensors. Widely available and affordable components are adopted for cost-effective production. It is shown through experiments that the proposed sensor covers over 97 % area of its surrounding sphere and it has a similar accuracy to a 32 channel Velodyne LIDAR sensor within its working range.

As a future work, we will apply the proposed sensor to small vehicles such as drones. In doing so, a rotating motor could be replaced with yawing motion of drones. Since the proposed sensor would be a good choice as a convenient and

economical 3D omnidirectional depth sensor, we believe that its myriad of applications are waiting to be developed.

REFERENCES

[1] S. Yang, X. Yi, Z. Wang, Y. Wang, and X. Yang, "Visual SLAM using multiple RGB-D cameras," in *Proc. IEEE Int. Conf. Robot. Biomimetics*, Dec. 2015, pp. 1389–1395.
[2] S. K. Nayar, "Catadioptric omnidirectional camera," in *Proc. IEEE Comput. Soc. Conf. Comput. Vis. Pattern Recognit.*, Jun. 1997, pp. 482–488.
[3] R. Orghidan, J. Salvi, and E. M. Mouaddib, "Modelling and accuracy estimation of a new omnidirectional depth computation sensor," *Pattern Recognit. Lett.*, vol. 27, no. 7, pp. 843–853, 2006.
[4] R. Marani, V. Renò, M. Nitti, T. D'Orazio, and E. Stella, "A compact 3D omnidirectional range sensor of high resolution for robust reconstruction of environments," *Sensors*, vol. 15, no. 2, pp. 2283–2308, 2015.
[5] D.-M. Córdova-Esparza, J.-J. Gonzalez-Barbosa, J.-B. Hurtado-Ramos, and F.-J. Ornelas-Rodriguez, "A panoramic 3D reconstruction system based on the projection of patterns," *Int. J. Adv. Robotic Syst.*, vol. 11, no. 4, p. 55, 2014.
[6] C. Zhang, J. Xu, N. Xi, Y. Jia, and W. Li, "Development of an omnidirectional 3D camera for robot navigation," in *Proc. IEEE/ASME Int. Conf. Adv. Intell. Mechatron.*, Jul. 2012, pp. 262–267.
[7] J. Xu, B. Gao, C. Liu, P. Wang, and S. Gao, "An omnidirectional 3D sensor with line laser scanning," *Opt. Lasers Eng.*, vol. 84, pp. 96–104, Sep. 2016.
[8] J. Iglesias, P. Mirado, and R. Ventura, "Towards an omnidirectional catadioptric RGB-D camera," in *Proc. IEEE/RSJ Int. Conf. Intell. Robots Syst.*, Oct. 2016, pp. 2506–2513.
[9] M. Bosse and R. Zlot, "Continuous 3D scan-matching with a spinning 2D laser," in *Proc. IEEE Int. Conf. Robot. Automat.*, May 2009, pp. 4312–4319.
[10] A. Nuchter, K. Lingemann, J. Hertzberg, and H. Surmann, "6D SLAM with approximate data association," in *Proc. Int. Conf. Adv. Robot.*, 2005, pp. 242–249.
[11] T. Fujita, "3D sensing and mapping for a tracked mobile robot with a movable laser ranger finder," *Int. J. Mech. Mechatron. Eng.*, vol. 6, no. 2, pp. 501–506, 2012.
[12] M. Sheehan, A. Harrison, and P. Newman, "Automatic self-calibration of a full field-of-view 3D n-laser scanner," in *Experimental Robotics*, O. Khatib, V. Kumar, and G. Sukhatme, Eds. Berlin, Germany: Springer, 2014, pp. 165–178.
[13] T. Ueda, H. Kawata, T. Tomizawa, A. Ohya, and S. Yuta, "Mobile sokuiki sensor system-accurate range data mapping system with sensor motion," in *Proc. IEEE Int. Conf. Auton. Robots Agents*, 2006, pp. 1–6.
[14] H. Qin, Y. Bi, F. Lin, Y. F. Zhang, and B. M. Chen, "A 3D rotating laser based navigation solution for micro aerial vehicles in dynamic environments," *Unmanned Syst.*, vol. 6, pp. 1–8, Sep. 2018.
[15] K. S. Kim and L. Sentis, "Human body part multicontact recognition and detection methodology," in *Proc. IEEE Int. Conf. Robot. Automat.*, May/Jun. 2017, pp. 1908–1915.
[16] D. Scaramuzza, A. Martinelli, and R. Siegwart, "A toolbox for easily calibrating omnidirectional cameras," in *Proc. IEEE/RS Int. Conf. Intell. Robots Syst.*, Oct. 2006, pp. 5695–5701.
[17] R. B. Fisher and D. K. Naidu, "A comparison of algorithms for subpixel peak detection," in *Image Technology: Advances in Image Processing, Multimedia and Machine Vision*. Berlin, Germany: Springer, 1996, pp. 385–404.
[18] D. Scaramuzza, A. Martinelli, and R. Siegwart, "A flexible technique for accurate omnidirectional camera calibration and structure from motion," in *Proc. 4th IEEE Int. Conf. Comput. Vis. Syst. (ICVS)*, Jan. 2006, p. 45.
[19] Z. Zhang, "A flexible new technique for camera calibration," *IEEE Trans. Pattern Anal. Mach. Intell.*, vol. 22, no. 11, pp. 1330–1334, 2000.
[20] K. Konolige, J. Augenbraun, N. Donaldson, C. Fiebig, and P. Shah, "A low-cost laser distance sensor," in *Proc. IEEE Int. Conf. Robot. Automat.*, May 2008, pp. 3002–3008.
[21] J. H. Gao and L.-S. Peh, "A smartphone-based laser distance sensor for outdoor environments," in *Proc. IEEE Int. Conf. Robot. Automat. (ICRA)*, May 2016, pp. 2922–2929.
[22] R. Mur-Artal and J. D. Tardós, "ORB-SLAM2: An open-source SLAM system for monocular, stereo, and RGB-D cameras," *IEEE Trans. Robot.*, vol. 33, no. 5, pp. 1255–1262, Oct. 2017.
[23] J. Morales, J. L. Martínez, A. Mandow, A. J. Reina, A. Pequeño-Boter, and A. García-Cerezo, "Boresight calibration of construction misalignments for 3D scanners built with a 2D laser rangefinder rotating on its optical center," *Sensors*, vol. 14, no. 11, pp. 20025–20040, 2014.

YOUNGBIN SON received the B.S. degree in computer science and engineering and the M.S. degree in electrical engineering from the Pohang University of Science and Technology (POSTECH), Pohang, South Korea, in 2013 and 2015, respectively, where he is currently pursuing the Ph.D. degree in creative IT engineering. His current research interests include sensor fusion, aerial robotics, and embedded systems.

SEONGWON YOON received the B.S. degree in electrical engineering and the M.S. degree in electrical engineering from KonKuk University, Seoul, South Korea, in 2014 and 2017, respectively. He is currently pursuing the Ph.D. degree in creative IT engineering with the Pohang University of Science and Technology (POSTECH), Pohang, South Korea. His research interests include robust optimal control systems for unmanned aerial vehicle (UAV) and stochastic signal processing.

SE-YOUNG OH received the B.S. degree in electronics engineering from Seoul National University, Seoul, South Korea, in 1974, and the M.S. and Ph.D. degrees in electrical engineering from Case Western Reserve University, Cleveland, OH, USA, in 1978 and 1981, respectively. From 1981 to 1984, he was an Assistant Professor with the Department of Electrical Engineering and Computer Science, University of Illinois at Chicago. From 1984 to 1988, he was an Assistant Professor with the Department of Electrical Engineering, University of Florida, Gainesville. In 1988, he joined the Department of Electrical Engineering, Pohang University of Science and Technology, Pohang, South Korea, where he is currently an emeritus professor. His research interests include neural networks, deep learning architecture, and evolutionary computation-based optimization and their applications to robotics, including intelligent vehicles and autonomous drones.

SOOHEE HAN received the B.S. degree in electrical engineering from Seoul National University (SNU), Seoul, South Korea, in 1998, and the M.S. and Ph.D. degrees from the School of Electrical Engineering and Computer Science, SNU, in 2000 and 2003, respectively. From 2003 to 2007, he was a Researcher with the Engineering Research Center for Advanced Control and Instrumentation, SNU. In 2008, he was a Senior Researcher with the Robot S/W Research Center. From 2009 to 2014, he was with the Department of Electrical Engineering, Konkuk University, Seoul, South Korea. Since 2014, he has been with the Department of Creative IT Engineering, Pohang University of Science and Technology, Pohang, South Korea.

His current research interests include computer aided control system designs, distributed control systems, time delay systems, and stochastic signal processing.